PAPER

Check for updates

"Catch and release" of the Cp^{N3} ligand using cobalt: dissociation, protonation, and C–H bond thermochemistry†

Sanju Luhach, [ID] Roger A. Lalancette and Demyan E. Prokopchuk [ID] *

The coordination chemistry of an amine-rich Cp^{N3} ligand has been explored with cobalt. We demonstrate that in the presence of NaCo(CO)$_4$, the cationic precursor **[Cp^{N3}]$^+$** yields the complex **Cp^{N3}Co^I(CO)$_2$**. While 2e$^-$ oxidation generates new Co^{III} complexes such as **[Cp^{N3}Co(NCMe)$_3$]$^{2+}$** and **Cp^{N3}CoI$_2$(CO)**, subsequent ligand loss is facile, generating free **[Cp^{N3}]$^+$** or the protonated dication **[Cp^{N3}H]$^{2+}$**. We have structurally characterized both these ligand release products *via* single crystal X-ray diffraction and obtained thermochemical C–H bond strengths *via* experiment and density functional theory (DFT). Upon reversible 1e$^-$ reduction, the radical cation **[Cp^{N3}H]$^{•+}$** has a weak C–H BDFE of 52 kcal mol^{-1} in acetonitrile. Mechanistic analysis shows that **[Cp^{N3}H]$^{•+}$** undergoes radical–radical disproportionation in the absence of exogenous H-atom acceptors, which is supported by deuterium isotope labelling experiments. Structural comparison of these organic molecules shows a high degree of iminium-like electron delocalization over the C–N bonds connected to the central five-membered ring.

Introduction

Cyclopentadienyl (Cp) ligands and derivatives thereof can be complexed to virtually all d-block metals and have been used extensively in homogeneous catalysis.[1–4] While Cp ligands are usually considered chemically "innocent", special cases arise where the ligand becomes chemically non-innocent, enabling Cp to act as a reservoir for protons (H$^+$), hydrogen atoms (H$^•$), and hydrides (H$^-$).[5] To this end, our group recently reported that an amine rich Cp^{N3} ligand coordinated to iron behaves as a proton acceptor, resulting in regiospecific *endo*-Cp^{N3} ring protonation as an essential step during electrocatalytic H$_2$ production.[6,7] To access these Fe(Cp^{N3}) compounds, an Fe^0 source such as Fe$_2$CO$_9$ reacts with vividly colored "cyclopentadienylium" cations ([**Cp^{N3}**]$^+$),[8] furnishing piano-stool [Fe^{II}(Cp^{N3})L$_3$]$^+$ salts.[7,9,10]

Cobalt complexes containing Cp ligands have also been explored for applications in chemical fuel synthesis and catalysis.[11–15] Notably, cyclopentadienylcobalt complexes **A** and **B** contain diphosphine ligands with bio-inspired pendant amines in their secondary sphere,[16–18] exhibiting electrocatalytic activity for H$_2$ production and CO$_2$-to-formate

reduction (Fig. 1).[19,20] In the proposed electrocatalytic cycles, the Cp ring remains chemically innocent while the nitrogen atoms in the secondary coordination sphere assist in proton transfer and/or proton-coupled electron transfer steps *en route* to product formation.

In our efforts to expand the library of M(Cp^{N3}) complexes that exhibit chemically non-innocent behavior, we now report the synthesis and reactivity of Co(Cp^{N3}) complexes **1** and **2**
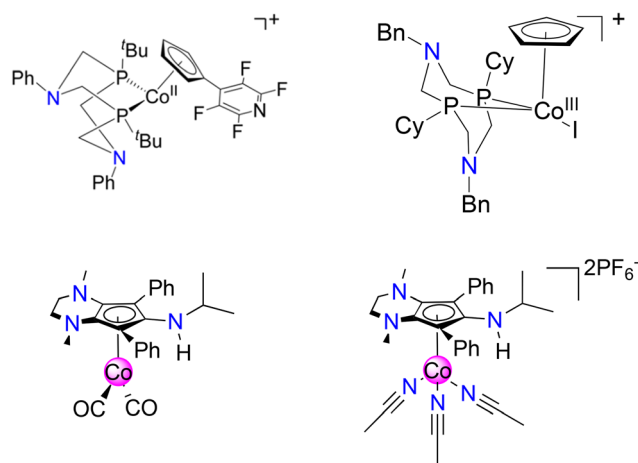

Fig. 1 Cyclopentadienylcobalt electrocatalyst system for H$_2$ production (**A**, top left)[19] and CO$_2$ reduction (**B**, top right)[20] containing pendant amines in secondary coordination sphere. This work: synthesis and reactivity of CoCp^{N3} complexes **1** (bottom left) and **2** (bottom right).

Department of Chemistry, Rutgers University-Newark, 73 Warren Street, Newark, NJ 07102, USA. E-mail: demyan.prokopchuk@rutgers.edu

(Fig. 1). While exploring their redox behavior and ligand substitution chemistry, we discovered that irreversible dissociation of $[Cp^{N3}]^+$ is facile and results in regiospecific ligand protonation at a carbon atom within the Cp^{N3} ring to yield the air stable organic dication $[Cp^{N3}H]^{2+}$. After independently synthesizing $[Cp^{N3}H]^{2+}$ *via* protonation of $[Cp^{N3}]^+$, we explore its C(sp³)–H bond thermochemistry in MeCN, enabling us to experimentally measure its redox potential ($E°$), C–H acidity (pK_a) and homolytic C–H bond dissociation free energy (BDFE). Our experimentally calculated data are supported by computational (DFT) analysis, and a comparison of single crystal X-ray diffraction data and DFT-derived molecular orbitals demonstrate the highly delocalized π electron distribution for the metal-free Cp^{N3} cations.

Results & discussion

The isopropyl-substituted cyclopentadienylium salt $[Cp^{N3}][BF_4]$, where $[Cp^{N3}]^+$ = 6-isopropyl-1,4-dimethyl-5,7-diphenyl-2,3,4,6-tetrahydrocyclopenta[*b*]pyrazin-6-ylium, was prepared using a previously reported procedure[8] and a more detailed description of ligand charge distribution will be described later using X-ray crystallographic data. Complex $Cp^{N3}Co(CO)_2$ (**1**) was prepared by refluxing $[Cp^{N3}]^+$ and NaCoCO$_4$[21] in toluene under N_2 and isolated as analytically pure orange crystals in 70% yield (Scheme 1). As anticipated, ¹H NMR spectroscopic analysis reveals that metal coordination enhances the electron density at the $[Cp^{N3}]^+$ ligand, causing the aliphatic isopropyl peaks to shift to 0.50 ppm *versus* 0.85 ppm in free ligand[22] dissolved in CD_3CN (Fig. S1†). Infrared spectral analysis shows strong carbonyl stretches at ν_{CO} = 1970 and 1901 cm⁻¹ (KBr) which are significantly lower than the analogous $CpCo(CO)_2$ (2028, 1967 cm⁻¹)[23] and (pentamethylcyclopentadienyl)cobalt(I) dicarbonyl, $Cp^*Co(CO)_2$ (2010, 1950 cm⁻¹; Cp^* = pentamethylcyclopentadienyl),[24] further demonstrating the increased electron density at cobalt in complex **1**. Single crystals of **1** suitable for X-ray diffraction show that the C–C bond distances within the Cp^{N3} ring of **1** are equidistant, lying between 1.42 and 1.46 Å (Fig. 2). The $[Cp^{N3}]^+$ ring binds to the metal center in an η⁵ coordination mode, formally oxidizing the Co^{I-} precursor
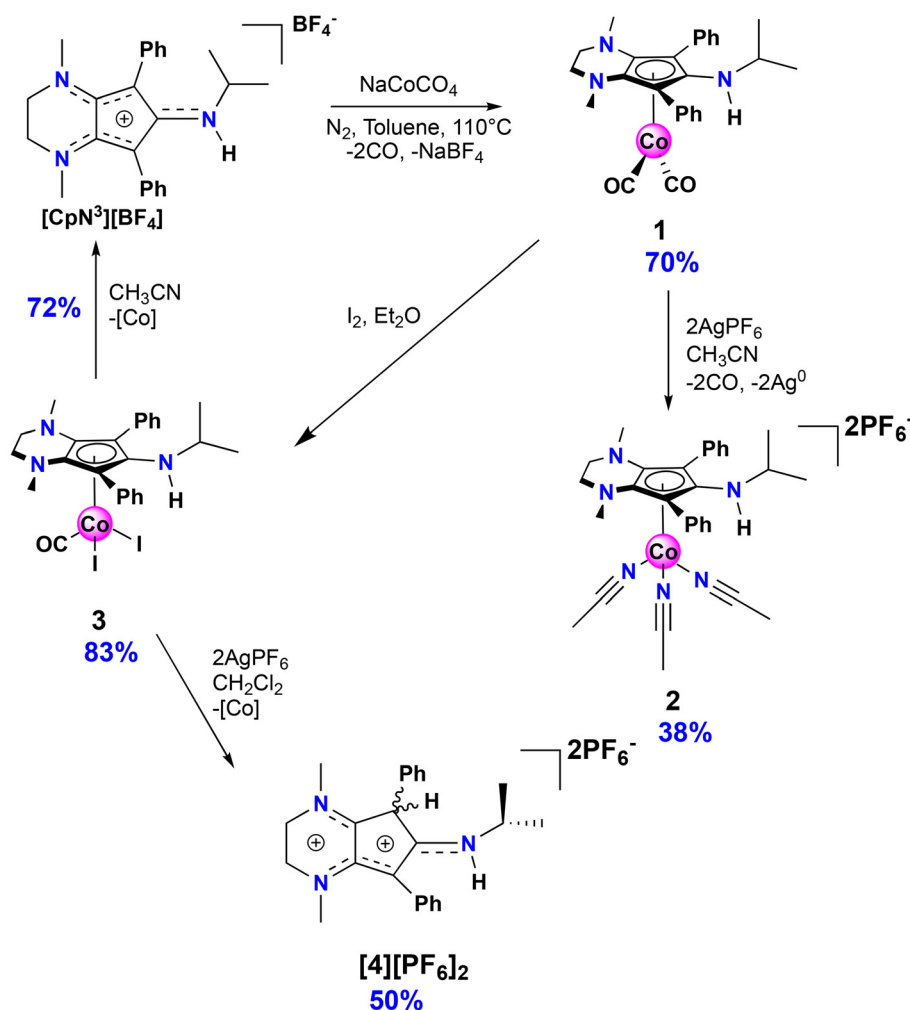
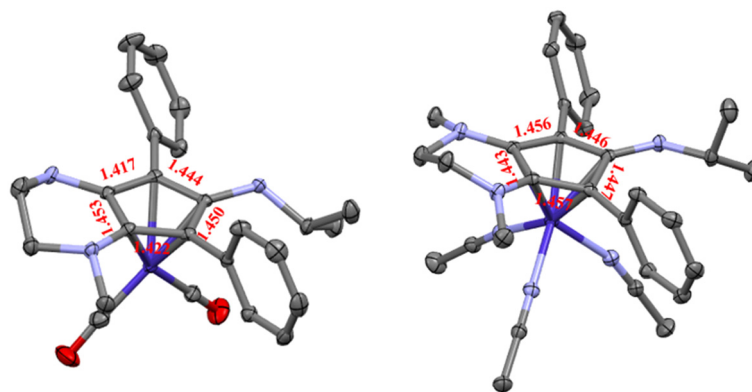**Scheme 1** Syntheses of compounds **1–4**.

Fig. 2 X-Ray crystallographic structures for complex **1** (left) and **2** (right) with 50% probability ellipsoids. Distances are shown in Angstroms (Å) and hydrogens/counteranions have been omitted for clarity.

by $2e^-$ and reducing the cationic $[\mathbf{Cp^{N3}}]^+$ by $2e^-$ upon coordination.

Electrochemical analysis of **1** *via* cyclic voltammetry (CV) in MeCN shows a redox wave at $E_{1/2}$ = 0.46 V *vs.* $Fc^{+/0}$ when starting at 0 V and sweeping in the anodic direction (Fig. 3). Further sweeping in the cathodic direction reveals an irreversible reduction at E_{pc} = −1.20 V followed by an oxidation peak at E_{pa} = −0.50 V *vs.* $Fc^{+/0}$. The observed oxidation and reduction peaks at −0.50 V and −1.20 V, respectively, are interdependent because the reduction peak does not appear if the voltage sweep is terminated before the oxidation event (Fig. S17†). Based on these observations, we hypothesize that $1e^-$ oxidation of **1** triggers a series of chemical events that lead to the formation of a new redox-active species centered at $E_{1/2}$ = 0.46 V with a corresponding reduction feature at −1.20 V *vs.* $Fc^{+/0}$. Using slower scan rates (100 mV s^{-1}) makes the minor features around −0.4 V and 0 V more prominent, suggesting that multi-step (electro)chemical processes are occurring in solution (Fig. S18†).
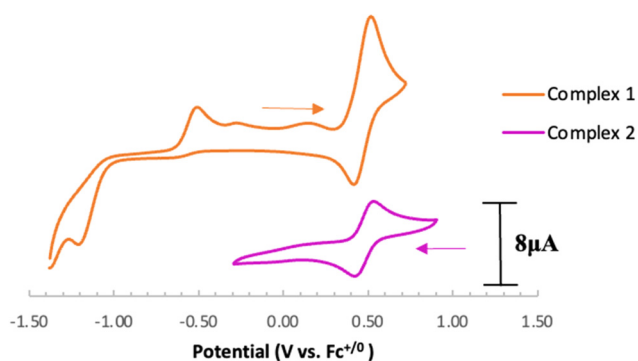
Based on the observed CV features for **1**, we pursued the chemical oxidation of **1** with a commercially available oxidant, $AgPF_6$ (E'° = 0.04 V, MeCN).[25] Upon mixing **1** and two equiv. $AgPF_6$ in MeCN, a fuchsia-colored solution formed, which after workup and X-ray crystallization revealed the tris-MeCN substituted Co^{III} complex $[\mathbf{Cp^{N3}Co(NCMe)_3}][\mathbf{PF_6}]_2$ (**2**) in 38% yield with concomitant CO release (Scheme 1 and Fig. 2). Notably, free ligand $[\mathbf{Cp^{N3}}]^+$ is formed as the major side-product as observed by ^1H NMR, and varying standard reaction optimization parameters (time, temperature, reagent concentrations, order of addition) does not change the product distribution. The crystalline product is obtained by slow diffusion of diethyl ether into a concentrated acetonitrile solution, however minor impurities also precipitate, precluding the isolation of analytically pure product (Fig. S3 and S4†). Paramagnetic impurities also appear to coprecipitate with the crystalline product, resulting in peak broadening in ^1H NMR spectra if single crystals are not adequately segregated from the powdered mixture. Using other oxidants such as "magic blue" (tris (4-bromophenyl) ammoniumyl hexafluoroantimonate) or $FcPF_6$ result in lower product yields and purities of **2**. However, to our delight, CVs of **2** in the cathodic direction reveal a redox wave at $E_{1/2}$ = 0.47 V, indicating a $Co^{III/II}$ redox couple which is consistent with our interpretation of the CV data for **1** (Fig. 3). Voltammograms collected beyond −0.72 V also reveal that unknown redox-active impurities are present in solution (Fig. S19†). Therefore, our synthetic and voltametric data show that the oxidation of **1** in acetonitrile leads to irreversible CO loss and formation of the isolable redox-active solvento complex **2**.

We pursued ligand substitution reactions using complex **2** in the presence of common bidentate ligands such as 1,2-bis (diphenylphosphino)ethane (dppe), 1,2-bis(diethylphosphino) ethane (depe), and bipyridne (bipy), hoping that solvent dissociation would lead to the formation of new complexes with the general formula $[\mathbf{Cp^{N3}Co(NCMe)L_2}]^{2+}$. In every case, clean and rapid ligand dissociation immediately generates $[\mathbf{Cp^{N3}}]^+$ in solution, and using dppe enabled us to crystallize the known Co^{II} bis(diphosphine) complex $[\mathbf{Co(dppe)_2(NCMe)}]^{2+}$.[26] These

Fig. 3 Cyclic voltammograms of complex **1** and **2** at 800 mV s^{-1}. Conditions: Ar, MeCN solvent, 0.1 M [Bu$_4$N][PF$_6$], 1.0 mM analyte, PEEK-encased glassy carbon working electrode, Type 2 glassy carbon rod counter electrode, Ag/AgCl pseudoreference electrode in a frit-separated (CoralPor) glass compartment containing solvent and electrolyte. Initial scan direction and starting position indicated with arrows.

results suggest that reduction of the metal center is thermo-dynamically and kinetically preferred, along with $2e^-$ oxidation and dissociation of $[\mathbf{Cp^{N3}}]^+$, instead of coordinating stronger σ-donor chelates to $Cp^{N3}Co^{III}$. Using a relatively electron-poor L-type donor, 2-isocyano-1,3-dimethylbenzene, also resulted in the formation of $[\mathbf{Cp^{N3}}]^+$.

Motivated by the success of using the diiodo reagent $CpCo^{III}I_2(CO)$ as a synthon for preparing new redox-active cobalt complexes,[11–13] exposure of **1** to I_2 in diethyl ether cleanly generates $\mathbf{Cp^{N3}CoI_2CO}$ (**3**) as an analytically pure brownish-black solid that precipitates from solution (Scheme 1). Similar to **1**, IR spectroscopic analysis shows a significantly more activated CO ligand (ν_{CO} = 2000 cm^{-1}, KBr) in **3** when compared to $CpCo^{III}I_2(CO)$ (2035 cm^{-1}).[27] Surprisingly, halide abstraction in the presence of $AgPF_6$ in DCM results in the clean and consistent release of *protonated* free ligand $[\mathbf{Cp^{N3}H}][\mathbf{PF_6}]_2$, ($[\mathbf{4}][\mathbf{PF_6}]_2$), a dicationic product containing a proton at the phenyl-substituted carbon of the Cp^{N3} ring (Scheme 1). Although air-free conditions were used in combination with thoroughly dried solvents and reagents, the origin of the proton remains unclear. A maximum yield of 50% suggests that partial decomposition may lead to the formation of $\mathbf{4^{2+}}$ (Scheme 1). The introduction of H^+ on the $[\mathbf{Cp^{N3}}]^+$ ring desymmetrizes the molecule and restricts free rotation about the C–N bond of the *N*-isopropyl moiety due to its enhanced iminium-like character, generating chemically inequivalent methyl resonances in NMR spectra (Fig. S5†). Gratifyingly, the BF_4^- salt of dication $\mathbf{4^{2+}}$ can be independently prepared in quantitative yield by simply protonating $[\mathbf{Cp^{N3}}]^+$ with $HBF_4 \cdot Et_2O$ in DCM, generating $[\mathbf{Cp^{N3}H}][\mathbf{BF_4}]_2$, ($[\mathbf{4}][\mathbf{BF_4}]_2$) (Scheme 2). Single crystals suitable for X-ray diffraction were obtained *via* vapor diffusion of diethyl ether into a concentrated acetonitrile solution and with metrical parameters revealing a delocalized positive charge distributed across three iminium-like N–C bonds and one alkene-like C–C bonds, respectively (Fig. 5 and Table 1). Moreover, dissolving complex **3** in MeCN releases *unprotonated* free ligand, $[\mathbf{Cp^{N3}}]^+$

Table 1 Selected bond lengths (Å) and bond angles (°) for $[\mathbf{Cp^{N3}}]^+$, $[\mathbf{Cp^{N3}H}]^{2+}$, $[\mathbf{Cp^{N3}H_2}]^+$

	$[\mathbf{Cp^{N3}}]^+$	$[\mathbf{Cp^{N3}H}]^{2+}$	$[\mathbf{Cp^{N3}H_2}]^+$
C(1)–C(2)	1.465(3)	1.516(2)	1.511(2)
C(2)–C(3)	1.368(4)	1.503(2)	1.556(2)
C(3)–C(4)	1.513(3)	1.467(2)	1.514(2)
C(4)–C(5)	1.373(4)	1.392(2)	1.414(2)
C(5)–C(1)	1.452(3)	1.420(2)	1.396(2)
C(1)–N(1)	1.314(3)	1.301(2)	1.326(2)
C(3)–N(2)	1.340(3)	1.284(2)	1.451(2)
C(4)–N(3)	1.341(3)	1.326(2)	1.308(2)
C(1)–C(2)–C(3)	105.4(2)	99.5(1)	100.5(1)
C(2)–C(3)–C(4)	108.5(2)	110.7(1)	102.9(1)
C(3)–N(2)–C(6)	121.0(2)	123.4(1)	110.7(1)
C(4)–N(3)–C(7)	121.8(2)	124.5(1)	123.1(1)
C(3)–C(4)–C(5)	109.2(2)	107.6(1)	109.0(1)
C(4)–C(5)–C(1)	105.1(2)	109.0(1)	107.5(1)
C(5)–C(1)–C(2)	111.1(2)	111.8(1)	112.6(1)
C(5)–C(1)–N(1)	127.9(2)	125.0(1)	124.7(1)

(Fig. S11†), and unidentified cobalt-containing byproducts suggesting that solvent identity plays some role in ligand protonation.

Intrigued by these results, we sought to study the C(sp^3)–H proton-coupled electron transfer (PCET) thermochemistry[28,29] of the protonated compound $[\mathbf{4}][\mathbf{BF_4}]_2$, as we have recently shown that $[\mathbf{Cp^{N3}}]^+$ ring protonation is essential during H_2 production electrocatalysis using $Cp^{N3}Fe(CO)_2$ complexes.[6,7] To determine the C(sp^3)–H bond acidity of $\mathbf{4^{2+}}$, we found *via* trial and error that reactions with aniline generate an equilibrium mixture of $\mathbf{4^{2+}}$, $[\mathbf{Cp^{N3}}]^+$, aniline, and anilinium BF_4^- (pK_a^{MeCN} = 10.62)[30–32] in solution (Fig. S9 and S10†). Using equilibrium ^1H NMR spectroscopic data at room temperature, we determined that the pK_a^{MeCN}(C–H) = 11.7 ± 0.1 for compound $\mathbf{4^{2+}}$ (see the ESI for details†). This experimentally derived pK_a is only four units more acidic than the computed C–H pK_a of 15.7 for the *endo*-protonated electrocatalytic intermediate $[(endo\text{-}Cp^{N3}H)Fe(NCMe)(CO)_2]^+$.[7] The CV of $[\mathbf{4}]^{2+}$ in MeCN
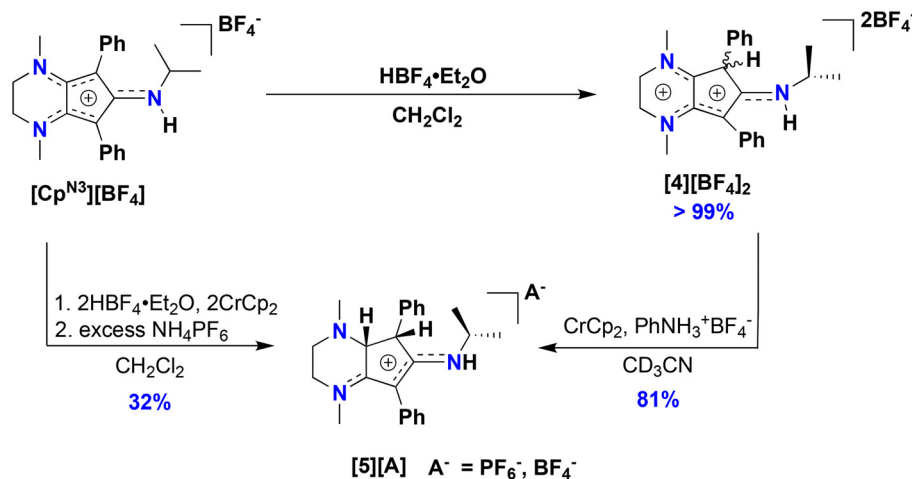
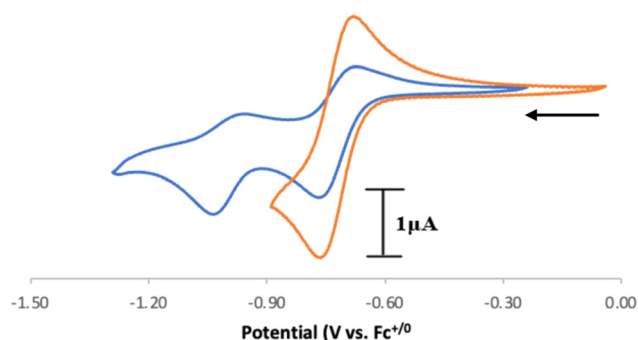**Scheme 2** Syntheses of compounds **4** and **5**.

Fig. 4 Cyclic voltammograms of $[4]^{2+}$ at 100 mV s^{-1}. The cathodic to anodic peak current ratio (i_{pa}/i_{pc}) is 0.47 when swept beyond −1.20 V and 0.76 when the scan direction is switched at −0.90 V. Conditions: Ar, MeCN solvent, 0.1 M [Bu$_4$N][PF$_6$], 1.0 mM analyte, PEEK-encased glassy carbon working electrode, Type 2 glassy carbon rod counter electrode, Ag/AgCl pseudoreference electrode in a frit-separated (CoralPor) glass compartment containing solvent and electrolyte. Initial scan direction and starting position indicated with an arrow.
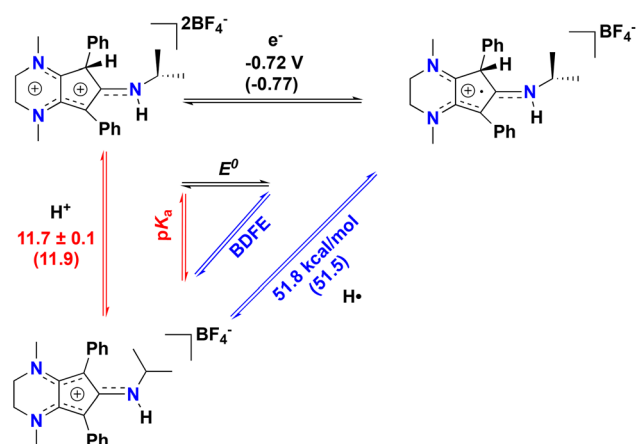
Scheme 3 PCET thermochemistry for $[Cp^{N3}]^+$, $[4]^{2+}$, and $[4]^{\cdot+}$ ^{a} (^{a} = DFT-computed values are in parentheses).

shows two partially reversible redox curves at *ca.* −0.72 V and −1.0 V *vs.* Fc$^{+/0}$ (Fig. 4). We surmise that the first reduction peak is 1e$^-$ reduction of $[4]^{2+}$ to the radical cation $[Cp^{N3}H]^{\cdot+}$ ($[4]^{\cdot+}$) while the second reduction yields the neutral Cp^{N3}H (**4**), neither of which we have been able to experimentally isolate to date. If the switching potential in CV experiments is set to −0.90 V, the first reduction becomes more reversible, with $E_{1/2}(4^{2+/+})$ = −0.72 V and i_{pa}/i_{pc} = 0.76. Using these data enables us to calculate the PCET thermochemistry for $[Cp^{N3}]^+$, $[4]^{2+}$, and $[4]^{\cdot+}$ as shown in Scheme 3. A weak C(sp^3)–H BDFE of 51.8 kcal mol^{-1} is determined for $[4]^{\cdot+}$ (Scheme 3), which is similar in magnitude to the M–H BDFEs of CpCr(CO)$_2$(PPh$_3$)H ^{28,33} (52.7 kcal mol^{-1}) and (dppm)V(CO)$_4$H ^{28,34} (51.1 kcal mol^{-1}) in MeCN. To further validate these data, the DFT calculated values in parentheses in Scheme 3 are in excellent agreement with experimental data (see the ESI for computational details†). We also computed the C–H pK_a of the radical cation $[4]^{\cdot+}$, which would generate the neutral radical species $[Cp^{N3}]^{\cdot}$ upon release of H$^+$. Our computations indicate that the decrease in overall charge increases the pK_a of $[4]^{\cdot+}$ to 26.2 in acetonitrile, making it about 14 orders of magnitude less acidic than $[4]^{2+}$.

We then turned our attention to studying the propensity of radical cation $[4]^{\cdot+}$ to undergo H-atom transfer (HAT) reactions, as organic radical cations have been widely used in synthetic organic transformations.[35] Reduction of $[4][BF_4]_2$ in the presence of one equiv. chromocene (Cp$_2$Cr; $E_{1/2}$ = −1.12 V *vs.* Fc$^+$/Fc^0) reveals a 1:1 ratio of $[Cp^{N3}]^+$ and a new organic compound *via* ^{1}H NMR spectroscopy (Fig. S12†). X-ray diffraction of colorless single crystals reveals this compound to be $[Cp^{N3}H_2][BF_4]$, ($[5][BF_4]$), where one of the diene moieties of Cp ring has been reduced (Scheme 2, Fig. 5 and 6). While the reduction of $[4]^{2+}$ using classic borohydride or aluminum hydride reagents resulted in intractable product mixtures, the hydrogenation product $[5][BF_4]$ can also be accessed *via* H$^+$/e$^-$ addition to $[4]^{2+}$, suggesting that H-atom transfer (HAT) is required to cleanly form $[5]^+$ (Scheme 2).

We propose that $[5][BF_4]$ forms through bimolecular HAT involving radical–radical disproportionation of $[4]^{\cdot+}$ to produce
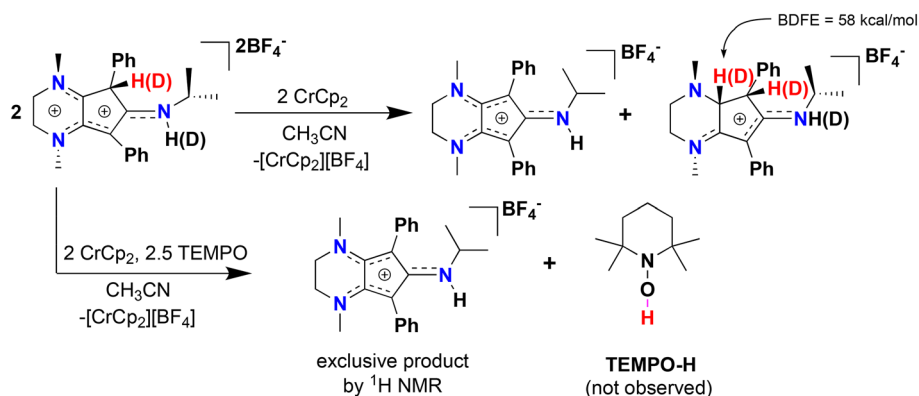

Fig. 5 Top: reductive disproportionation of $[Cp^{N3}H][BF_4]_2$ ($[4][BF_4]_2$) to give $[Cp^{N3}]^+$ and $[Cp^{N3}H_2][BF_4]$ ($[5][BF_4]$) with a computed BDFE of 58 kcal mol^{-1} for the newly formed C−H bond. Bottom: reduction in the presence of excess TEMPO.

equimolar amounts of **[5][BF₄]** and **[Cp^N3]⁺**. To support this hypothesis, we prepared the deuterated analogue **[Cp^N3D][BF₄]₂** by adding two drops of MeOD to a stirring solution of **[4][BF₄]₂** in CD₃CN, resulting in 95% H–D exchange at

the ring carbon and full deuteration of the secondary amine (Fig. 5 and Fig. S13†). Addition of 1 equiv. chromocene to this product results in the deuteration at one additional site within the Cp ring of **[5][BF₄]**, which is wholly consistent with an
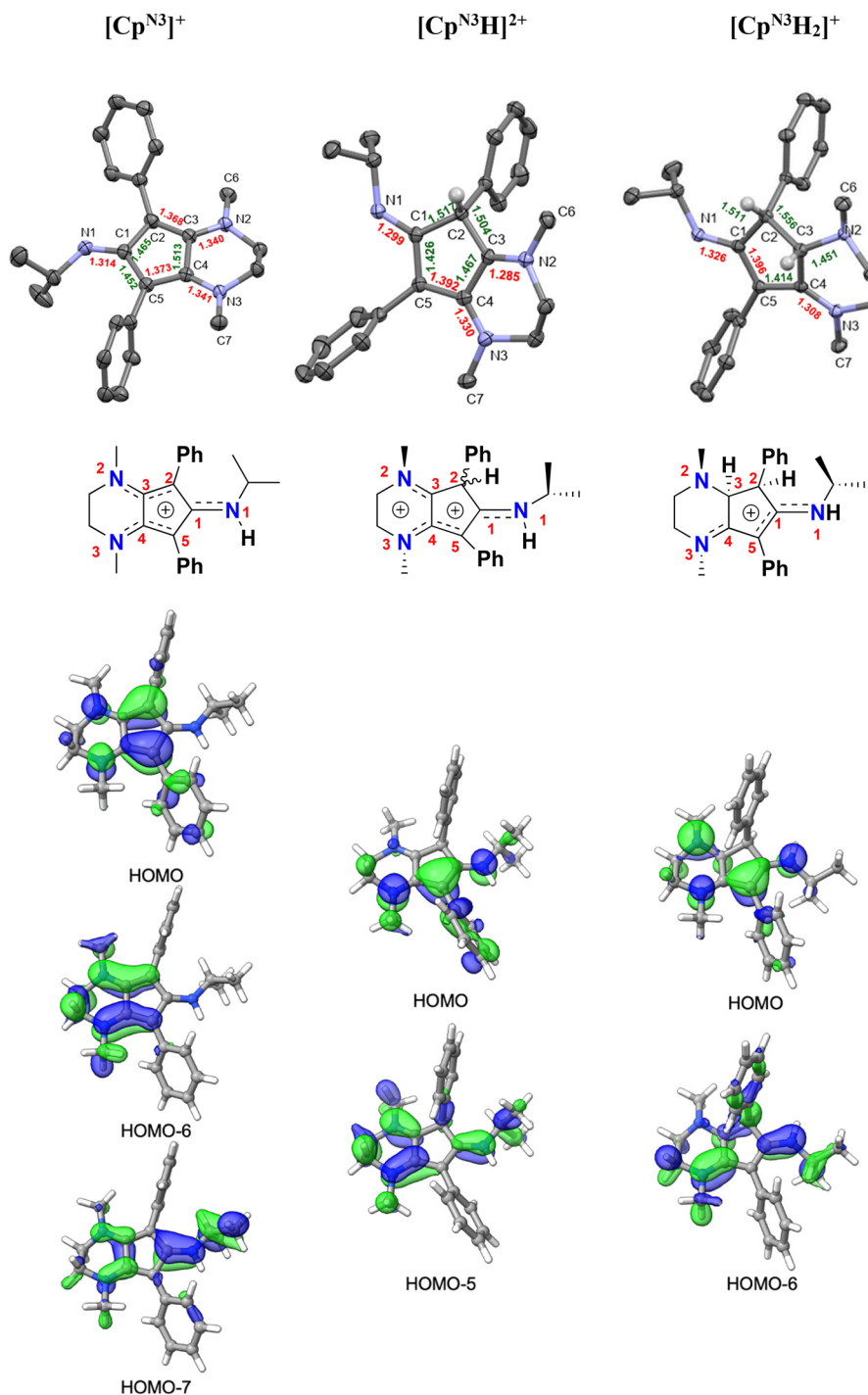

Fig. 6 Top: X-ray crystallographic structures of **[Cp^N3][B(C₆F₅)₄]** (left), **[Cp^N3H][BF₄]₂** (**[4][BF₄]₂**, middle), and **[Cp^N3H₂][PF₆]** (**[5][PF₆]**; right) with 50% probability ellipsoids. Co-crystallized solvent molecules, counterions, and most hydrogens have been omitted for clarity. Middle: structural cartoons showing charge delocalization based on metrical parameters and typical interatomic distances for organic compounds (see Table 1 and discussion). Bottom: selected molecular orbitals for all three molecules, showing the main π-type MOs responsible for electron delocalization involving the Cp^N3 ring (isovalue = 0.04).

intermolecular HAT event (Fig. S14 and S15†). Moreover, DFT calculations support the feasibility of HAT to $[5]^+$ *via* $[4]^{•+}$ on thermochemical grounds, as the BDFE(C–H) for $[5]^+$ is calculated to be 58.0 kcal mol^{-1}. We then tried this same reaction in the presence of TEMPO, expecting that the weak C(sp^3)–H BDFE of 51.8 kcal mol^{-1} for $4^{•+}$ would quantitatively generate TEMPO-H (BDFE(O–H) = 66 kcal mol^{-1}, MeCN)^{36} and $[\mathbf{Cp^{N3}}]^+$. However, with only one equiv. TEMPO and Cp$_2$Cr in solution, a 3 : 1 ratio of $[\mathbf{Cp^{N3}}]^+ : [5]^+$ is observed suggesting that the kinetics of bimolecular HAT are comparable to the HAT kinetics involving TEMPO. Gratifyingly, reacting $[\mathbf{4}][\mathbf{BF_4}]_2$ with 5 equiv. TEMPO and one equiv. Cp$_2$Cr does exclusively generate $[\mathbf{Cp^{N3}}]^+$ *via* ^{1}H NMR spectroscopy (Fig. 5 and S16†), although we could not clearly identify signals belonging to TEMPO-H in these spectra. Furthermore, compound $[5]^+$ can be independently synthesized *via* 2H$^+$/2e$^-$ reduction of $[\mathbf{Cp^{N3}}]^+$ and isolated as the PF$_6^-$ salt ($[\mathbf{Cp^{N3}H_2}][\mathbf{PF_6}]$) in 32% yield (Scheme 2, Fig. S7 and S8†).

In addition to having X-ray structural data for $[\mathbf{4}]^{2+}$ and $[5]^+$, we were also fortunate to obtain X-ray quality crystals of $[\mathbf{Cp^{N3}}]^+$ *via* anion exchange with B(C$_6$F$_5$)$_4^-$, enabling us to compare the metrical parameters for all three salts with respect to typical interatomic distances for organic compounds (Fig. 6 and Table 1).^{37,38} Crystallographic analysis of $[\mathbf{Cp^{N3}}]^+$ indicates that C(2)–C(3) and C(4)–C(5) are far closer to an average C$_{sp^2}$=C$_{sp^2}$ bond length (1.330 Å) while C(1)–C(2), C(3)–C(4) and C(5)–C(1) are more consistent with singly-bonded C$_{sp^2}$–C$_{sp^2}$ atoms (1.460 Å). Moreover, the C–N bonds to the five-membered ring are all substantially shorter than expected for C$_{sp^2}$–N$_{sp^3}$ atoms (1.468 Å) and harbor more C=N double bond character when compared to typical C1$_{sp^2}$=N1$_{sp^2}$ distances (1.301 Å). These combined factors lead us to depict the positive charge delocalization of $[\mathbf{Cp^{N3}}]^+$ with dashed lines in all Figures and Schemes throughout this article. Similarly in case of $[\mathbf{4}]^{2+}$, C(4)–C(5) bond distances match well with average C$_{sp^2}$=C$_{sp^2}$ bond lengths (1.330 Å) while C(1)–C(5) and C(3)–C(4) are closer to an average singly-bonded C$_{sp^2}$–C$_{sp^2}$ atoms (1.460 Å). The bond lengths for C(3)–N(2) C(4)–N(3) and C(1)–N(1) are closer to typical C$_{sp^2}$=N$_{sp^2}$ distances (1.301 Å). For $[5]^+$, C(1)–N(1) and C(4)–N(3) have a C$_{sp^2}$=N$_{sp^2}$ double bond character (1.301 Å) and the C(5)–C(1) bond lengths are closer to average literature C$_{sp^2}$=C$_{sp^2}$ (1.330 Å) distance. Molecular orbital DFT analyses generally agree with this assessment (Fig. 6, bottom). There are three low-lying π-type MOs mainly responsible for the delocalized electron density in $[\mathbf{Cp^{N3}}]^+$ (HOMO, HOMO−6, HOMO−7), two MOs in $[\mathbf{4}]^{2+}$ (HOMO, HOMO−5), and two MOs in $[5]^+$ (HOMO, HOMO−6).

Conclusion

In summary, we have prepared new Co(Cp^{N3}) complexes that either undergo CO loss upon oxidation or $[\mathbf{Cp^{N3}}]^+$ ligand dissociation. Upon loss of cobalt, we observe selective protonation at the five-membered Cp^{N3} ring to give $[\mathbf{Cp^{N3}H}]^{2+}$, which was independently prepared in high yield *via* protonation of $[\mathbf{Cp^{N3}}]^+$. Through equilibrium measurements *via* ^{1}H NMR spectroscopy and cyclic voltammetry, we experimentally determined the C(sp^3)–H pK_a and $[\mathbf{Cp^{N3}H}]^{2+}/[\mathbf{Cp^{N3}H}]^{•+}$ redox potential. Using these data, we calculated the C–H BDFE of $[\mathbf{Cp^{N3}H}]^{•+}$, which has a very weak BDFE in MeCN (52 kcal mol^{-1}). Although H-atom transfer in the presence of excess TEMPO is feasible with *in situ* 1e$^-$ reduction of $[\mathbf{Cp^{N3}H}]^{2+}$, attempts to isolate this radical cation in the absence of an H-atom acceptor result in radical disproportionation to give diamagnetic products $[\mathbf{Cp^{N3}H_2}]^+$ and $[\mathbf{Cp^{N3}}]^+$. With the help of single-crystal X-ray diffraction data, we were able to compare the structural parameters of all three Cp^{N3} salts, showing that positive charge delocalization is distributed across the iminium-like C–N bonds. Work is ongoing to explore the reactivity of these Cp^{N3} salts in the presence and absence of 3d metals.

Data availability

The CCDC contains the supplementary crystallographic data for entries 2358580–2358584.† Additional raw data is available from the authors upon request.

Conflicts of interest

There are no conflicts of interest to declare.

Acknowledgements

References

1 P. J. Chirik, *Organometallics*, 2010, **29**, 1500–1517.
2 J. Mas-Roselló, A. G. Herraiz, B. Audic, A. Laverny and N. Cramer, *Angew. Chem.*, 2021, **133**, 13306–13332.
3 P. J. Shapiro, *Coord. Chem. Rev.*, 2002, **231**, 67–81.
4 M. Enders and R. W. Baker, *Curr. Org. Chem.*, 2006, **10**, 937–953.
5 A. VanderWeide and D. E. Prokopchuk, *Nat. Rev. Chem.*, 2023, **7**, 561–572.
6 B. Goel, H. Neugebauer, A. I. VanderWeide, P. Sánchez, R. A. Lalancette, S. Grimme, A. Hansen and D. E. Prokopchuk, *ACS Catal.*, 2023, **13**, 13650–13662.
7 P. Sánchez, B. Goel, H. Neugebauer, R. A. Lalancette, S. Grimme, A. Hansen and D. E. Prokopchuk, *Inorg. Chem.*, 2021, **60**, 17407–17413.
8 R. Gompper and H. Glöckner, *Angew. Chem., Int. Ed. Engl.*, 1984, **23**, 53–54.

9 A. Lator, Q. G. Gaillard, D. S. Mérel, J.-F. Lohier, S. Gaillard, A. Poater and J.-L. Renaud, *J. Org. Chem.*, 2019, **84**, 6813–6829.

10 Q. G. Gaillard, L. Bettoni, D. Paris, C. Lequertier, J. F. Lohier, S. Gaillard and J. L. Renaud, *Adv. Synth. Catal.*, 2023, **365**, 3704–3712.

11 A. W. Cook, T. J. Emge and K. M. Waldie, *Inorg. Chem.*, 2021, **60**, 7372–7380.

12 K. M. Waldie, S. Ramakrishnan, S.-K. Kim, J. K. Maclaren, C. E. Chidsey and R. M. Waymouth, *J. Am. Chem. Soc.*, 2017, **139**, 4540–4550.

13 K. M. Waldie, S. K. Kim, A. J. Ingram and R. M. Waymouth, *Eur. J. Inorg. Chem.*, 2017, **2017**, 2755–2761.

14 U. Koelle and S. Paul, *Inorg. Chem.*, 1986, **25**, 2689–2694.

15 D. A. Kurtz, D. Dhar, N. Elgrishi, B. Kandemir, S. F. McWilliams, W. C. Howland, C.-H. Chen and J. L. Dempsey, *J. Am. Chem. Soc.*, 2021, **143**, 3393–3406.

16 R. M. Evans, E. J. Brooke, S. A. Wehlin, E. Nomerotskaia, F. Sargent, S. B. Carr, S. E. Phillips and F. A. Armstrong, *Nat. Chem. Biol.*, 2016, **12**, 46–50.

17 B. Mondal, J. Song, F. Neese and S. Ye, *Curr. Opin. Chem. Biol.*, 2015, **25**, 103–109.

18 M. Frey, *ChemBioChem*, 2002, **3**, 153–160.

19 M. Fang, E. S. Wiedner, W. G. Dougherty, W. S. Kassel, T. Liu, D. L. DuBois and R. M. Bullock, *Organometallics*, 2014, **33**, 5820–5833.

20 S. Roy, B. Sharma, J. Pécaut, P. Simon, M. Fontecave, P. D. Tran, E. Derat and V. Artero, *J. Am. Chem. Soc.*, 2017, **139**, 3685–3696.

21 J.-J. Brunet, C. Sidot and P. Caubere, *J. Organomet. Chem.*, 1981, **204**, 229–241.

22 A. Lator, Q. G. Gaillard, D. S. Merel, J.-F. Lohier, S. Gaillard, A. Poater and J.-L. Renaud, *J. Org. Chem.*, 2019, **84**, 6813–6829.

23 T. Piper, F. Cotton and G. Wilkinson, *J. Inorg. Nucl. Chem.*, 1955, **1**, 165–174.

24 L. R. Byers and L. F. Dahl, *Inorg. Chem.*, 1980, **19**, 277–284.

25 N. G. Connelly and W. E. Geiger, *Chem. Rev.*, 1996, **96**, 877–910.

26 R. Ciancanelli, B. C. Noll, D. L. DuBois and M. R. DuBois, *J. Am. Chem. Soc.*, 2002, **124**, 2984–2992.

27 R. King, *Inorg. Chem.*, 1966, **5**, 82–87.

28 R. G. Agarwal, S. C. Coste, B. D. Groff, A. M. Heuer, H. Noh, G. A. Parada, C. F. Wise, E. M. Nichols, J. J. Warren and J. M. Mayer, *Chem. Rev.*, 2021, **122**, 1–49.

29 D. D. Wayner and V. D. Parker, *Acc. Chem. Res.*, 1993, **26**, 287–294.

30 S. Tshepelevitsh, A. Kütt, M. Lõkov, I. Kaljurand, J. Saame, A. Heering, P. G. Plieger, R. Vianello and I. Leito, *Eur. J. Org. Chem.*, 2019, 6735–6748.

31 I. Kaljurand, A. Kütt, L. Soováli, T. Rodima, V. Mäemets, I. Leito and I. A. Koppel, *J. Org. Chem.*, 2005, **70**, 1019–1028.

32 F. G. Bordwell, *Acc. Chem. Res.*, 1988, **21**, 456–463.

33 G. Kiss, K. Zhang, S. L. Mukerjee, C. D. Hoff and G. C. Roper, *J. Am. Chem. Soc.*, 1990, **112**, 5657–5658.

34 J. Choi, M. E. Pulling, D. M. Smith and J. R. Norton, *J. Am. Chem. Soc.*, 2008, **130**, 4250–4252.

35 M. Schmittel and A. Burghart, *Angew. Chem., Int. Ed. Engl.*, 1997, **36**, 2550–2589.

36 C. F. Wise, R. G. Agarwal and J. M. Mayer, *J. Am. Chem. Soc.*, 2020, **142**, 10681–10691.

37 F. H. Allen, O. Kennard, D. G. Watson, L. Brammer, A. G. Orpen and R. Taylor, *J. Chem. Soc., Perkin Trans. 1*, 1987, S1–S19.

38 A. G. Orpen, L. Brammer, F. H. Allen, O. Kennard, D. G. Watson and R. Taylor, *J. Chem. Soc., Dalton Trans.*, 1989, S1–S83.